New Journal and we have not received input yet 24 (2020) 100209

Contents lists available at ScienceDirect

FlatChem

journal homepage: www.sciencedirect.com/journal/flatchem

Boosting Li-S battery performance by an efficient polysulfide double-blocking strategy

Pengfei Lu [a], Haodong Shi [a,c], Jieqiong Qin [a,c], Zhong-Shuai Wu [a,b,*]

[a] State Key Laboratory of Catalysis, Dalian Institute of Chemical Physics, Chinese Academy of Sciences, 457 Zhongshan Road, Dalian 116023, China
[b] Dalian National Laboratory for Clean Energy, Chinese Academy of Sciences, 457 Zhongshan Road, Dalian 116023, China
[c] University of Chinese Academy of Sciences, 19 A Yuquan Rd, Shijingshan District, Beijing 100049, China

ARTICLE INFO

Keywords:
Lithium-sulfur battery
Cathode
CoS_2 interlayer
Polysulfides
Shuttling effect

ABSTRACT

Lithium-sulfur (Li-S) batteries have proven their merits for promising high-energy-density batteries. However, the notorious shuttling of polysulfides severely hinders their widespread applications. Herein, we report an efficient polysulfide double-blocking strategy that simultaneously employs the in-situ formed sulfur encapsulated in porous carbon materials (S@C) as cathode and metal-organic framework-derived CoS_2 nanosheets as polar interlayer to fabricate highly-stable Li-S batteries. The S particles with high loading of 71% are uniformly confined within the large voids and cavities of porous carbon skeleton, and the carbon shell could control the cathodic volume, ensure the fast ionic transfer, and physically confine the polysulfides. Further, the nanosheet-like CoS_2 interlayer presents strong chemical adsorption of polysulfides, as confirmed by the experiments and DFT calculations. As a result, the strong synergistic effect of S@C cathode and CoS_2 interlayer yields superior Li-S batteries with high initial capacity (1271 mAh g^{-1} at 0.5 C), remarkably enhanced rate capability and excellent cyclability with a quite low fading rate of 0.136% per cycle. Therefore, our proposed strategy of double blocking polysulfides will offer new ways for achieving high-stable and long-lifetime Li-S batteries.

1. Introduction

With the ever-increasing demand of 3C electronics, electric vehicles and large-scale grid applications, it is crucial to develop high-energy-density batteries with long cycling stability [1–6]. Among them, lithium-sulfur (Li-S) batteries have drawn considerable attention owing to the low-cost abundant sulfur reserves, high theoretical capacity (1675 mAh g^{-1}) and large specific energy density (2600 Wh kg^{-1}). However, it is still not primed for the state-of-the-art Li-S battery to be widely used and commercialized due to several drawbacks, such as the electrical insulation of elemental sulfur (5×10^{-28} S/m) and discharge products (Li_2S/Li_2S_2), large volumetric expansion, shuttle effect of polysulfides and lithium dendrites during cycling [7–10], leading to poor cycling life, significant capacity attenuation and low Coulombic efficiency for Li-S batteries.

To deal with these issues, tremendous efforts have been devoted to developing appropriate sulfur hosts and a certain level improvement of performance has been observed [11–17]. For example, porous carbon is a particularly promising sulfur host material for cathode design, not only because of superior electrical conductivity and large internal surface, which improves sulfur utilization, but also the confinement of porous carbon framework, which traps the nano-sized sulfur particles and increases the cathode stability [18,19]. However, it is worth noting that, confining polar polysulfides by only weak van der Waals force between S and C species is usually not enough to effectively suppress the shuttling of polysulfides over long-term cycling [20], serious capacity decay usually occurs when the sulfur content reaches 70% (in mass) or above.

Recently, lots of metallic oxides [21–23], sulfides [24–29], carbide [30] and nitrides [31–35] have been developed to anchor the polysulfides and enhance the cyclability of Li-S batteries owing to their strong polarities and high electrical conductivities. In particular, it is reported that CoS_2 can chemically adsorb the polysulfides by forming Li-S or S-Co bond when used in cathode of Li-S batteries [26,27]. By introducing CoS_2 nanosheets into the conductive porous carbon/sulfur cathode, the formed interfaces between CoS_2 and electrolyte can serve as efficient adsorption and activation sites for polar polysulfides to accelerate their redox reactions, resulting in enhanced capacity and cycling stability. Alternatively, the addition of one barrier interlayer

* Corresponding author at: State Key Laboratory of Catalysis, Dalian Institute of Chemical Physics, Chinese Academy of Sciences, 457 Zhongshan Road, Dalian 116023, China.
E-mail address: wuzs@dicp.ac.cn (Z.-S. Wu).

https://doi.org/10.1016/j.flatc.2020.100209
Received 23 September 2020; Received in revised form 3 November 2020; Accepted 9 November 2020
Available online 13 November 2020

between the separator and cathode is considered as another important strategy in Li-S batteries which can block the migration of polysulfides and prevent the shuttling effect during electrochemical processes [36–41]. So far, different barrier layers have been reported, such as carbon materials [42], metal oxides/hydroxides/carbides [43,44], conductive polymers [36,38].

As aforementioned above, the electrochemical performance of Li-S batteries could be improved by introducing polar adsorbents in the cathode or adding a blocking layer between cathode and separator. Therefore, one of the most promising strategies is the design and full construction of the carbon/sulfur cathode and interlayer together, which can work together with a strong synergistic effect with physical confinement and chemical adsorption of lithium polysulfides to further improve the performance. For example, Balach et al. assembled Li-S batteries with S cathode and N/S-codoped mesoporous carbon modified Celgard separator [45]. The N/S-codoped mesoporous carbon effectively inhibited polysulfide diffusion across the separator *via* both physical confinement and chemical adsorption, and therefore remarkably improved the performance with high capacity of 5.9 mAh cm^{-2} and ultralow capacity degradation of 0.041% per cycle. Similarly, polyacrylonitrile (PAN) and ammonium polyphosphate (APP) were electrospun into a multifunctional separator (PAN@APP), which displayed strong binding interactions with polysulfides [36]. Combined with traditional S/C cathodes, the Li-S battery demonstrated a capacity retention of 83% over 800 cycles. Recently, Li et al. adopted the double-shelled hollow nanocages of N-doped carbon decorated with cobalt nitride (Co_4N) catalyst as the S host [46]. The carbon shell improved the electrical conductivity of the electrode and served as a physiochemical absorber for polysulfides. Importantly, Co_4N nanoparticles embedded in nitrogen-doped carbon efficiently catalyzed the conversion of polysulfides. As a result, the electrode showed large reversible capacity (1242 mAh g^{-1} at 0.1C) and robust stability (capacity retention of 658 mAh g^{-1} at 5 C after 400 cycles).

According to these reported works, the sulfur component is usually loaded into the interior of carbon host by melt-diffusion, during which some nano sulfur particles would deposit on the outer surface of porous carbon leading to serious dissolution in the electrolyte. The new strategy to prepare superior cathode with uniformly distributed sulfur in the carbon shell is necessary. On the other hand, polar CoS_2 material is an efficient adsorbent for polysulfides, but the potential of the CoS_2 interlayer is not explored fully for Li-S batteries. Therefore, in this work, an efficient polysulfide double-blocking strategy was developed for high-performance Li-S batteries, in which the in-situ formed sulfur encapsulated in porous carbon materials (S@C) was fabricated as cathode and metal–organic framework (MOF)-derived CoS_2 nanosheets was designed as a polar interlayer to physically confine and chemically adsorb lithium polysulfides. The strong synergistic effect of S@C cathode and CoS_2 interlayer produced outstanding performance for Li-S batteries, showing a high initial capacity of 1271 mAh g^{-1} at 0.5 C, and remarkably enhanced rate capability and cyclability with an extremely low fading rate of 0.136% per cycle.

2. Experimental section

2.1. Preparation of the S@C and S/CNT hybrids

The S@C hybrid was prepared by in-situ oxidation reaction [47]. Firstly, 5.0 g NaCl, 2.0 g Na_2S and 0.6 g glucose were put into about 20 mL deionized water and stirred for several minutes until completely dissolved. Then, the solution was treated with liquid nitrogen and deprived of water by freeze-drying to form the solid mixtures. After that, the resultant solid was ground into powder and heated at 750℃ for 2 h under an Ar atmosphere. Subsequently, the obtained black powder was added into 150 mL $Fe(NO_3)_3$ solution and stirred for 40 h to dissolve the NaCl and complete the reaction between Fe^{3+} and S^{2-}. Finally, the product was washed 3 times by distilled water and collected by filtration, which was defined as S@C-0.6. What's more, the hybrids with different amounts of glucose (1.0 g and 0.4 g) in the initial mixing step were defined as S@C-1.0 and S@C-0.4, respectively. For comparison, we also prepared the S/CNT hybrid by the melt-diffusion method [48]. A certain amount of CNT and S powder were thoroughly mixed by ball-milling process, ensuring the S content was no less than that of S@C-0.6. Then, the mixture was kept at 155 °C for 12 h in an enclosed glass tube under Ar atmosphere to facilitate the diffusion and encapsulation of melted sulfur into the CNT. Finally, the resultant S/CNT hybrid was collected for the cathode preparation.

2.2. Preparation of CoS_2 nanosheet interlayer

First, CoS_2 was synthesized in term of a previous work [49]. Briefly, 0.58 g $Co(NO_3)_2{\cdot}H_2O$ was mixed with 1.31 g 2-methylimidazole in 80 mL deionized water and stirred at room temperature for 4 h. After filtration and drying processes, the Co-MOF product was collected for subsequent sulfuration reaction. The prepared Co-MOF was mixed with 40 mL of thioacetamide (TAA, 1.2 g) and heated at 85℃ for 2 h under magnetic stirring. Then, the CoS_2 nanosheet was obtained by centrifugation, washing and calcinations (450 °C, 2 h). Second, the obtained CoS_2 nanosheets were filtrated onto the polypropylene (PP) separator to form the CoS_2 nanosheet interlayer. Typically, 0.8 mg CoS_2 nanosheet and polyvinylidene fluoride (PVDF) mixture (mass ratio: 10:1) was dispersed in a mixed solution of water (20 mL) and methanol (20 mL), and sonicated for 1 h. Then the solution was filtered on PP separator by vacuum filtration. The mass loading of CoS_2 was about 0.6 mg/cm^2.

2.3. Materials characterization

Morphologies of porous carbon host were disclosed by scanning electron microscopy (SEM, JSM-7800F), the microstructures of cathode materials and interlayer were explored by transmission electron microscope (TEM, JEM-2100) and the crystalline phase was further confirmed by high-resolution TEM (HRTEM, JEM-2100). The structures were also explored by X-ray diffraction (XRD, Empyrean with Cu Kα radiation) in the 2θ range from 10 to 70°. The sulfur content was explored by thermogravimetric analysis (TGA, NETZSCH STA 449 F3) and bonding information was disclosed by X-ray photoelectron spectroscopy equipment (XPS, Thermo ESCALAB 250Xi).

2.4. Electrochemical measurement

For the cathode, eight sets obtained S@C-1.0, S@C-0.6 or S@C-0.4 hybrid was mixed with one set conductive carbon, one set PVDF binder and several drops of N-methyl-2-pyrrolidone (NMP) in the mortar to form the slurry followed by casting step on the carbon-coated Al foil (200 μm in thickness). When the whole membrane was dried, the S cathode was obtained. Combined with CR2016 coin cells, CoS_2/PP separator, Li foil (0.5 mm in thickness) anode and 60 μL of Li-S electrolyte (with 1.0 M LiTFSI and 0.1 M $LiNO_3$ dissolved in the 1,3-dioxolane (DOL) and 1, 2-dimethoxymethane (DME) mixed solvent), the Li-S cells (defined as S@C-1.0//CoS_2/PP, S@C-0.6//CoS_2/PP, S@C-0.4//CoS_2/PP) were fabricated in the glove box filled with Ar. In addition, the batteries based on the S@C-0.6 (S/CNT hybrid) and PP separator was also fabricated and defined as S@C-0.6(S/CNT)//PP. For the electrochemical measurements, the electrochemical workstation (CHI 760E) was used for cyclic voltammetry (CV) test, the voltage range was set to 1.7 and 2.8 V (vs Li^+/Li) and the scanning rate was 0.1 mV/s. Electrochemical impedance spectra (EIS) tests were carried out (CHI 660D workstation) with the AC amplitude of 5 mV and the frequency range of 100 kHz to 0.01 Hz. In addition, by using LAND CT2001A, the galvanostatic charge and discharge (GCD) cycles were tested at constant temperature of 25 ℃. The specific capacity was calculated based on the areal mass of sulfur loaded in different sulfur cathodes.

2.5. Density functional theoretical calculations

The binding energies between polysulfide and CoS_2, polysulfide and PP were calculated and compared. The CoS_2 periodic slab model was constructed for CoS_2 and the propylene trimer model represented PP molecule. With Vienna Ab-initio Simulation Package (VASP), the density functional theory (DFT) calculations were conducted [50,51]. The generalized gradient approximation and Perdew-Burke-Enzerhof (GGA-PBE) functional were employed to deal with the electron exchange and correlation interactions [52,53]. The structural relaxations of CoS_2 and PP models were conducted firstly to obtain the minimal-energy structures. The cut-off energy of 400 eV was used. The minimum allowed energy change between the two adjacent iterative steps was set to 1×10^{-5} eV, and the tolerance of force was 0.05 eV/Å. Based on Monkhorst-Pack method [54], the Brillouin zone integration was sampled with $4 \times 4 \times 1$ and $1 \times 1 \times 1$ k-point grids for CoS_2 and PP models, respectively. The binding energy (E) was defined as the energy difference between the substrate model with the adsorbed molecule (E_{total}) and the summation of the adsorbed molecule (E_1) and substrate system (E_2): $E = E_{total} - (E_1 + E_2)$.

3. Results and discussion

The scheme of preparation for S@C cathode and CoS_2 nanosheet interlayer for Li-S batteries were shown in Fig. 1. First, the aqueous solution including Na_2S, glucose, and NaCl was freeze-dried followed by calcination at 750 °C, leading to the conversion of glucose to porous carbon. Then NaCl was washed out and simultaneously the S element in porous carbon was in-situ formed by the oxidation reaction of Na_2S with Fe^{3+} ions. By this in situ method, the S element could be evenly distributed and well wrapped by the carbon shell. It is worth noting that the S contents can be adjusted by simply changing the initial mass ratio of Na_2S to glucose. The existence of sulfur was confirmed by XRD pattern which presents the peaks at 2θ of 23.1°, 25.9° and 27.8°, corresponding to the (222), (026) and (040) planes of S crystal (JCPDS card no. 08-0247) [55]. By TGA, the amount of sulfur could be further quantitated as 28%, 55%, and 71% for S@C-1.0, S@C-0.6 and S@C-0.4, respectively (Fig. 2a, 2b and S1). The S amount in S/CNT hybrid was also measured as 65% as shown in Fig. S2. Therefore, based on the TGA test, the mass loadings of sulfur were calculated as 0.29, 0.53, 0.68 and 0.63 mg/cm^2 for S@C-1.0, S@C-0.6, S@C-0.4 and S/CNT cathodes, respectively. From SEM and TEM images (Fig. 2c-2f), 3D micro/mesoporous carbon can be easily observed. The S particles were effectively wrapped by carbon shell, which ensures the high utility of S element during the electrochemical processes. Moreover, the energy-dispersive X-ray spectroscopy (EDX) elemental mapping suggested the uniform distribution of sulfur in the porous carbon (Fig. 2g-2i).

Second, the MOF derived CoS_2 nanosheets were prepared by low-temperature (85 °C) hydrothermal sulfuration of Co-MOF nanosheets (Fig. S3), followed by annealing treatment at 450 °C for 2 h. The XRD pattern confirmed the successful preparation of CoS_2 (JCPDS card NO. 65-3322) nanosheets (Fig. 3a) [55]. The SEM and TEM images validated the formation of CoS_2 with the thickness of ~30 nm and the size of 200 ~ 500 nm, which well maintained the nanosheet-like structure of Co-MOF nanosheet (Fig. 3b and 3c). HRTEM image showed the well lattice fringe of CoS_2 nanosheet (Fig. 3d). Afterwards, the CoS_2 nanosheet interlayer on PP separator was obtained by vacuum filtration of the solution of CoS_2 nanosheets with a small amount of PVDF binder (10% of the CoS_2 in mass) on PP separator (the mass loading was about 0.6 mg/cm^2). From the SEM images (Fig. 3e, 3f), it is found that the porous CoS_2 layer was stacked by CoS_2 sheets, which provided large surface areas and abundant ion channels. SEM images confirmed the presence of the uniformly compact CoS_2 layer on the surface of pristine PP separator, and the thickness of the CoS_2 interlayer was about 7.5 μm. Importantly, the CoS_2 nanosheets/PP (CoS_2/PP) separator could retain high stability and flexibility under mechanical bending (Fig. 3f).

To demonstrate the critical role of CoS_2/PP separator in the performance improvement, the Li–S batteries S@C-0.6//CoS_2/PP and S@C-0.6//PP were compared. Fig. 4a and 4b display the initial three CV curves of Li–S batteries with and without MOF-CoS_2 interlayer

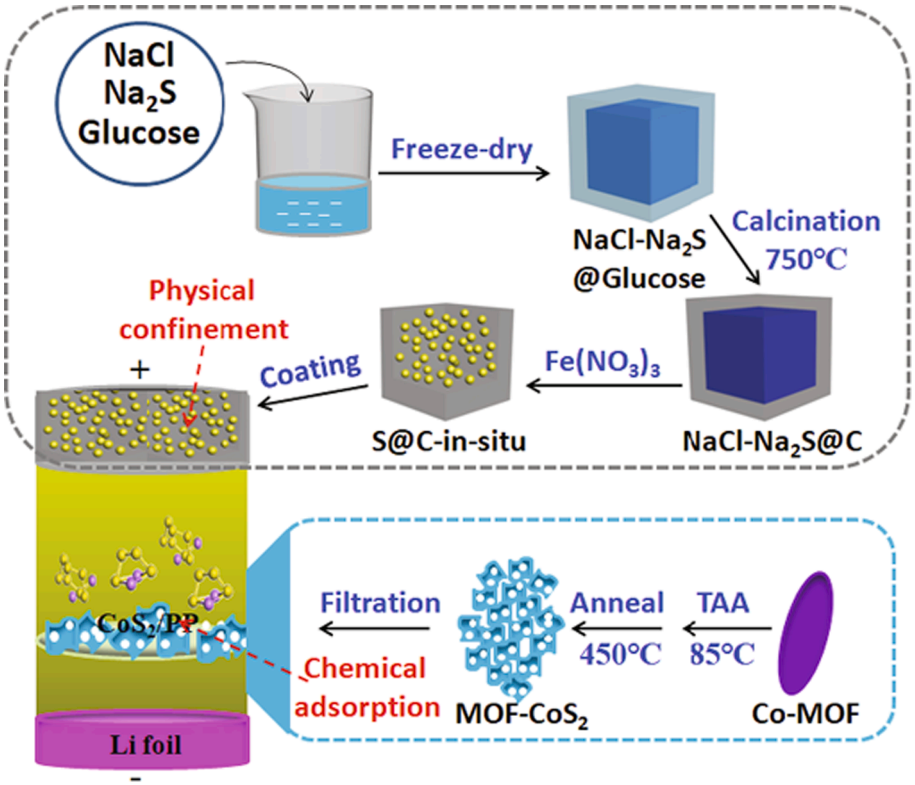

Fig. 1. Scheme of fabrication of S@C cathode and MOF-CoS_2 nanosheet interlayer for Li-S batteries.

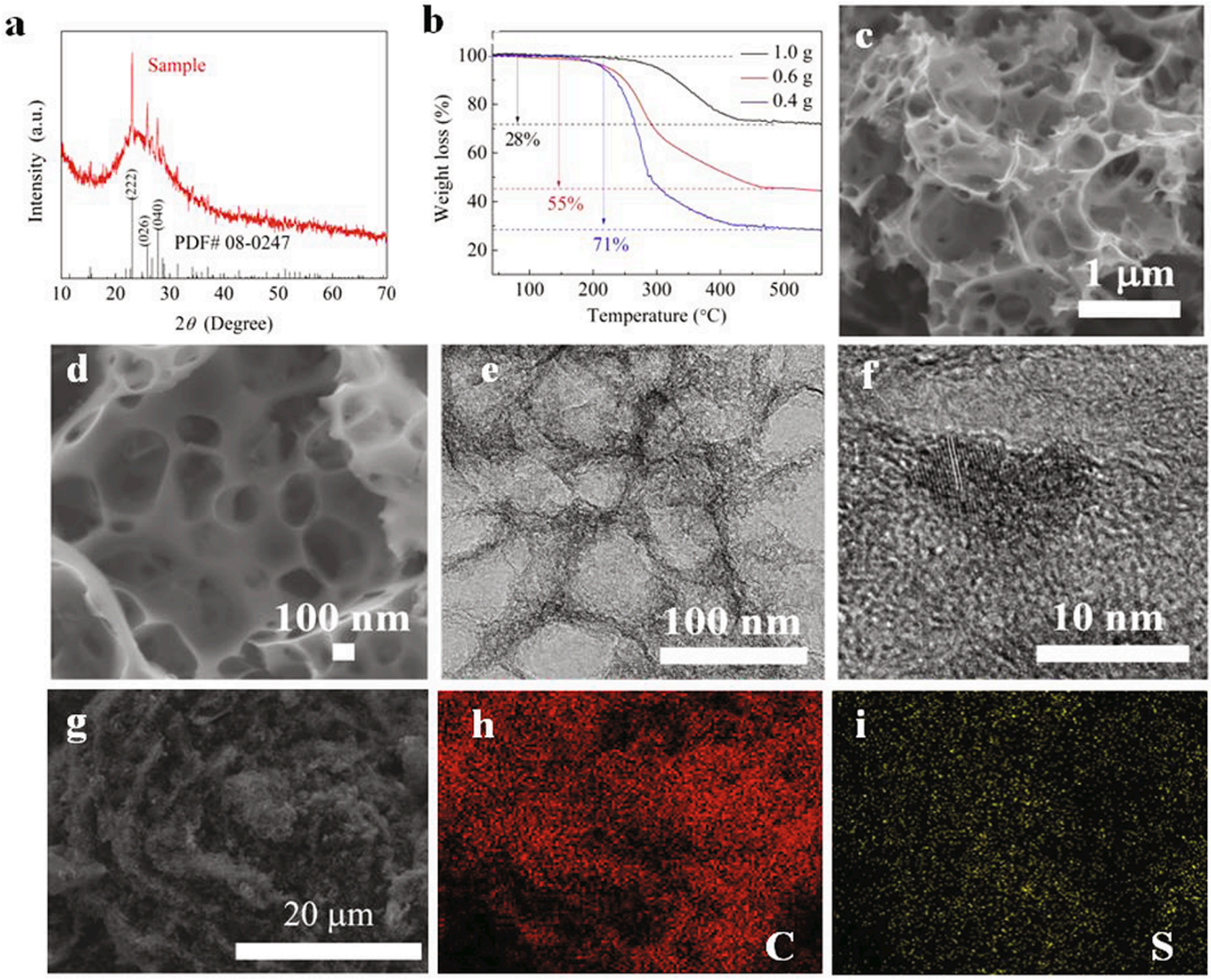

Fig. 2. Structure and morphology of in-situ formed S@C hybrid. (a) XRD pattern of S@C hybrid. (b) TGA profiles of S@C with the different contents of glucose. (c, d) SEM images of 3D porous carbon shell. (e, f) TEM and HRTEM images of S@C hybrid. (g-i) SEM image of S@C hybrid, and the corresponding C and S elemental mapping.

respectively. With CoS_2 interlayer, Li-S batteries showed the negligible current changes and potential shifts, and their shapes are almost overlapped, indicative of high electrochemical reversibility. However, without using CoS_2 interlayer, obvious evolution of both current and potential was observed. Further, Fig. 4c compared the first CV curve of Li–S batteries with and without CoS_2 interlayer. The Li-S battery with CoS_2 interlayer displayed two typical reduction peaks at 2.3 and 2.1 V in the cathodic scan, with the peak currents of 0.3 and 0.7 mA, respectively, which were attributed to the formation of long-chain lithium polysulfides (Li_2S_{4-8}) and short-chain Li_2S_2/Li_2S, respectively [56]. While for S@C-0.6//PP, the two reduction peaks appeared at the lower potentials (2.2 and 1.9 V) with the lower peak currents (0.2 and 0.5 mA), it was possibly attributed to the inferior conversion kinetics of the polysulfides aggregating near the cathode [32]. Despite, the traditional Li-S battery S/CNT//PP (65% S content in S/CNT) was also tested. The corresponding Li-S batteries also displayed the narrower profiles and lower peak currents (0.1 and 0.4 mA) at the cathodic scan, compared with S@C-0.6//CoS_2/PP (Figs. S4 and S5). Therefore, it was suggested that the superior battery performance was attribute to both the in-situ formed S@C cathode and the MOF-CoS_2 interlayer.

In addition, EIS plots were depicted in Fig. 4d, which displayed a semi-circle in the high and middle frequency ranges and an inclined line in the low frequency range, which demonstrated similar reaction processes for the batteries with and without CoS_2 interlayer. The batteries based on S@C-0.6//CoS_2/PP showed a lower interfacial resistance (20 Ω) than S@C-0.6//PP (35 Ω). It was similar to the Li-S batteries with other interlayers reports, in which the MOF-CoS_2 interlayer on PP separator enlarged the separator thickness, resulting less ion mobile in the separator, especially for the large polysulfide ions [57]. Meanwhile, the polar CoS_2 can provide more effective contact sites, which is beneficial to improve the adsorption and conversion of polysulfides [26,27,58].

To further highlight the superiority of the CoS_2 interlayer and S@C cathode, GCD tests were conducted. In the case of S@C-0.6//CoS_2/PP (Fig. 5a), GCD profiles of 3rd, 10th, 20th, 30th, 50th and 100th circles delivered the capacities of 1293, 1287, 1197, 1267, 1135 and 1019 mAh g^{-1}, respectively. While the capacity for S@C-0.6//PP sharply decreased from 1366 mAh g^{-1} at the 3rd cycle to 675 mAh g^{-1} at the 100th cycle (Fig. 5b). Fig. 5c further compared the GCD profiles at the third cycle, S@C-0.6// CoS_2/PP displayed a voltage gap of 197 mV between charge and discharge plateaus at 0.5C, which is narrower than that of S@C-0.6//PP (216 mV). The result indicated that the introduction of conductive MOF-CoS_2 interlayer is highly helpful for the conversion of polysulfides, which is consistent with the result in CV curves (Fig. 4c).

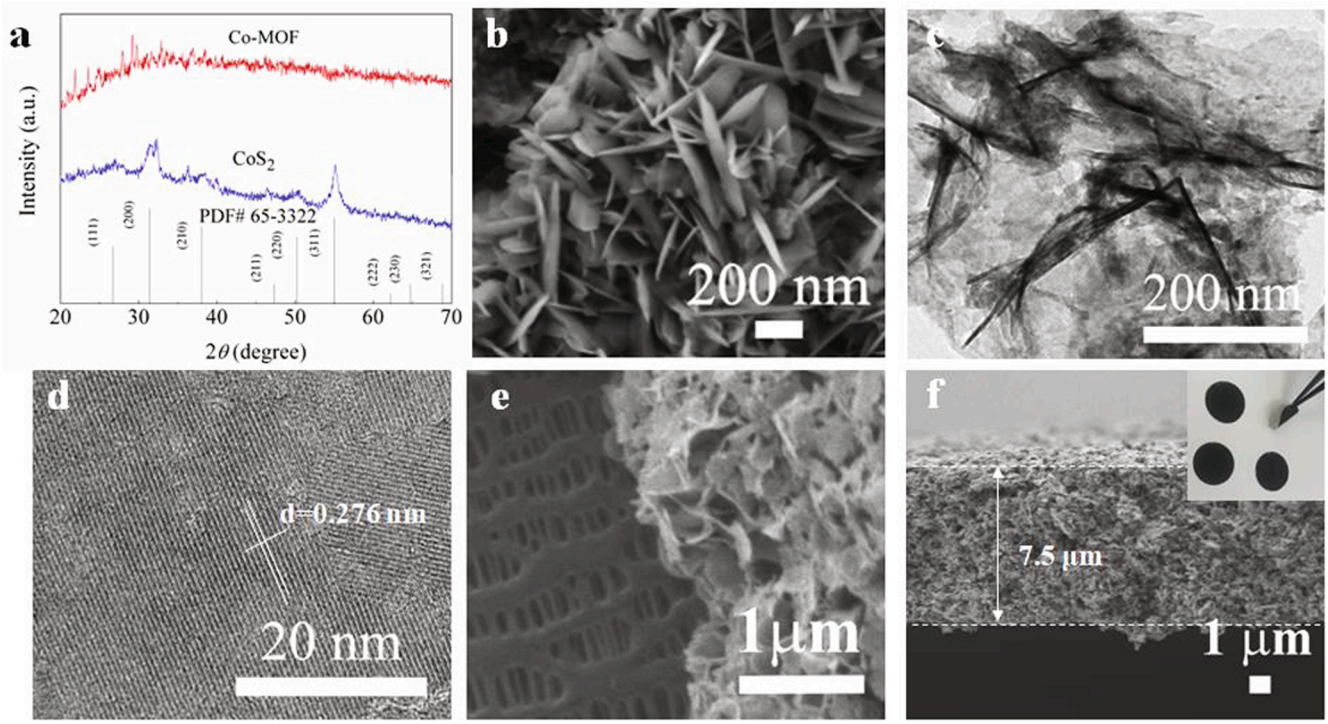

Fig. 3. Structure and morphology of MOF derived CoS_2 nanosheets. (a) XRD patterns of Co-MOF and MOF-derived CoS_2 nanosheets. (b, c) SEM and TEM images of CoS_2 nanosheets. (d) HRTEM image of CoS_2 nanosheet. (e) SEM image of PP separator with partially coated CoS_2 nanosheet. (f) Cross-section SEM image of CoS_2 nanosheet interlayer (Inset: Photographs of flexible CoS_2/PP separator).

For the cycling performance at 0.5C (Fig. 5d), S@C-0.6//CoS_2/PP delivered a little lower initial discharge capacity of 1271 mAh/g, but the capacity was well maintained. The fading rate is about 0.136% per cycle and the Coulombic efficiency is more than 99%. In comparison, S@C-0.6//PP based batteries given higher initial discharge capacity (1450 mAh g^{-1}), but sharply decreased during the 300 cycles, showing a fast capacity fading rate of about 0.242% per cycle. The Coulombic efficiency was about 98%. The Li-S batteries based on S/CNT//PP (65% and 55% S content in S/CNT) displayed extremely low capacity of ~420 mAh g^{-1} after 150 cycles (Figs. S6 and S7). More importantly, Li-S batteries with S@C cathode and CoS_2 interlayer also showed better rate performance, as shown in Fig. 5e. For S@C-0.6//CoS_2/PP, the battery delivered high reversible capacities of 1653 (0.2 C), 1189 (0.5 C), 831 (1 C), and 623 mAh g^{-1} (2 C), while lower capacities of 885 (0.2 C), 622 (0.5 C), 556 (1 C), and 497 mAh g^{-1} (2 C) were found for S@C-0.6//PP based batteries. In addition, the traditional Li-S batteries S/CNT//PP (65% S content in S/CNT) displayed better rate capability, but quite lower capacities of 716 (0.2 C), 471 (0.5 C), 388 (1 C), and 291 mAh g^{-1} (2 C), compared with S@C-based cathode for Li-S batteries (Fig. S8). Furthermore, the cycling performance of Li-S batteries based on different S@C cathodes were depicted in Fig. S9, in which S@C-1.0 presented lower S content (28%) and capacity compared with the others. S@C-0.4 with higher S content of 71% behaved similar stability to S@C-0.6. Notably, the high capacity for Li-S batteries with both S@C cathode and CoS_2 interlayer was well comparable to other Li-S cells reported (Table S1), such as the Li-S batteries with N/S-co-doped mesoporous carbon interlayer [45], MOF/nafion hybrids interlayer [38], PPy/ZnO interlayer [57], and so on.

To disclose the superior blocking effect of CoS_2 on polysulfides, the adsorptions of S_8 and polysulfides (Li_2S_n, n = 8, 6, 4, 2, 1) on CoS_2 and PP were theoretically studied. Owing to the polarity of CoS_2, S_8 and polysulfides could firmly bond to the CoS_2 surface with the adsorb energies of −0.285, −1.282, −1.274, −1.642, −2.289, and −0.718 eV, respectively, which were about 10 ~ 20 times higher than those on PP models (-0.022, −0.044, −0.104, −0.061, −0.160, and −0.095 eV) (Fig. 6a). The results theoretically confirmed the suppression effect of CoS_2 interlayer on the polysulfides shuttling..

The visual evidence was also obtained by conducting permeation test in optically transparent H-type glass cells. Briefly, Li_2S (36.8 mg) and S (128 mg) powders were mixed in 80 mL of tetrahydrofuran (THF) solvent. Then 20 mL prepared Li_2S_6 solution was poured into the left side of the glass cell while 20 mL THF in the other side. CoS_2/PP or PP separator was sandwiched between the two solutions. Under the force of concentration gradient, the polysulfides were able to penetrate the PP separator to the empty THF side and the color change occurred quickly from colorless to yellow, while there only appears a pale yellow color after 20 h for the CoS_2/PP case (Fig. 6b). These results further confirmed that the CoS_2 interlayer could significantly suppress the diffusion of polar polysufides in the separator by both the physical confinement and chemisorption.

To further assess the adsorption ability of CoS_2 to polysulfides, XPS was used to identify the bonding characteristics and the surface composition of CoS_2 before and after soaking in the Li_2S_6/THF solution. For the pristine CoS_2, the S2p XPS spectra showed three fitted peaks corresponding to S-Co (168.5 eV), S_2^{2-} (162.5 eV) and S^{2-} (161.4 eV) [59], indicative of the stable Co-S bonding (Fig. 6c). After being soaked in the Li_2S_6 solution, the S^{2-} and S_2^{2-} peaks shifted towards lower binding energy of 161.2 and 162.1 eV with the newly generated S-Li peak at 163.1 eV, indicative of the electron transfer between S atom of CoS_2 and Li atom. The results indicated that CoS_2 could adsorb lithium polysulfides (LiPSs) by forming strong Li-S chemical bond, which could greatly mitigate the LiPSs shuttling. In brief, it is suggested from both the experiments and DFT calculations that Li-S batteries with both S@C cathode and CoS_2 interlayer displayed superior performance to those with S@C-cathode and S/CNT-cathode. Further, S@C-cathode also showed better performance than S/CNT-cathode. It is demonstrated that the polysulfides could be effectively blocked by carbon shell of the in-situ formed S@C hybrid and meanwhile strongly adsorbed by the polar CoS_2 layer, in which the synergistic effect of S@C cathode and CoS_2 nanosheet interlayer played the key role in performance

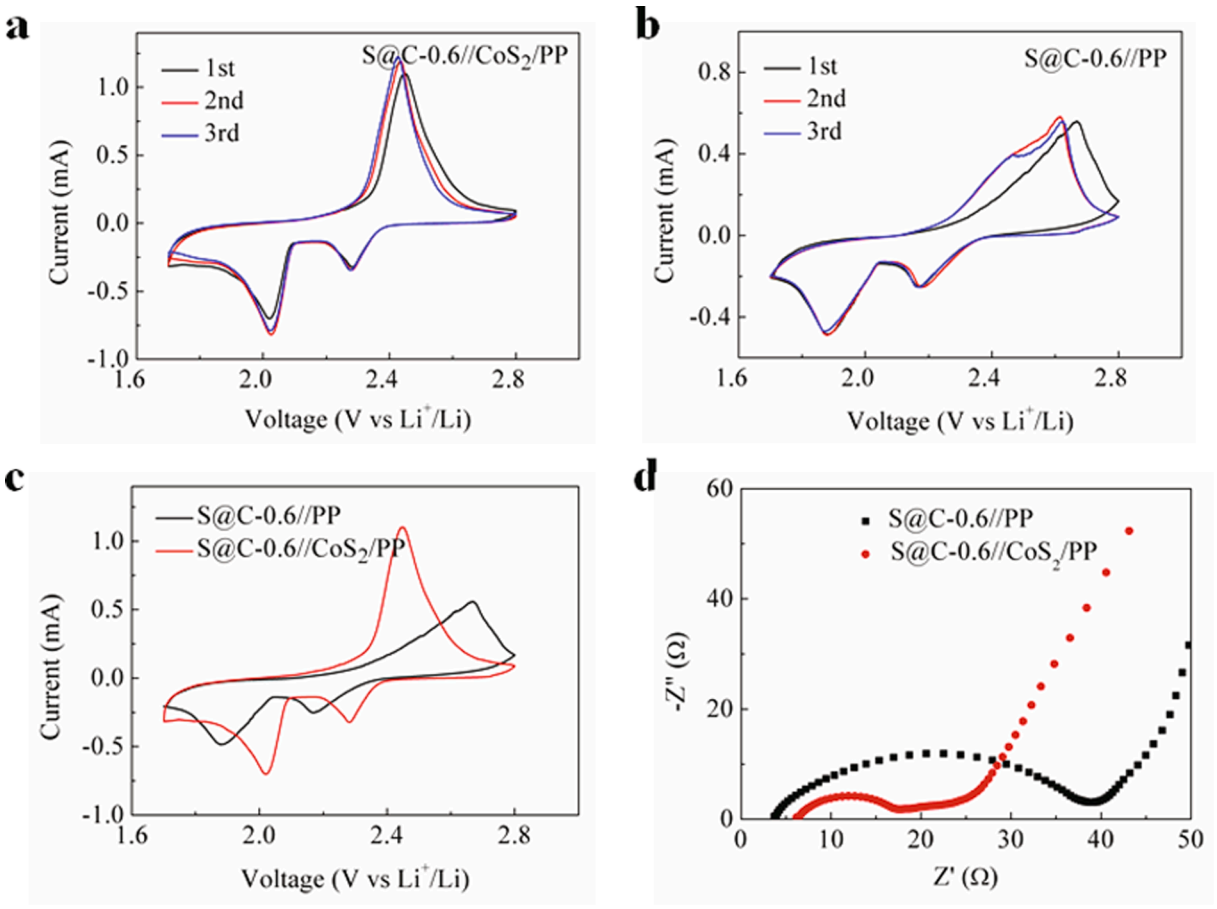

Fig. 4. Electrochemical performance of Li-S batteries S@C-0.6//CoS_2/PP and S@C-0.6//PP. (a, b) CV curves obtained at the initial three cycles. (c) CV curves comparison of Li-S batteries at the first cycle. (d) EIS of S@C-0.6//CoS_2/PP and S@C-0.6//PP.

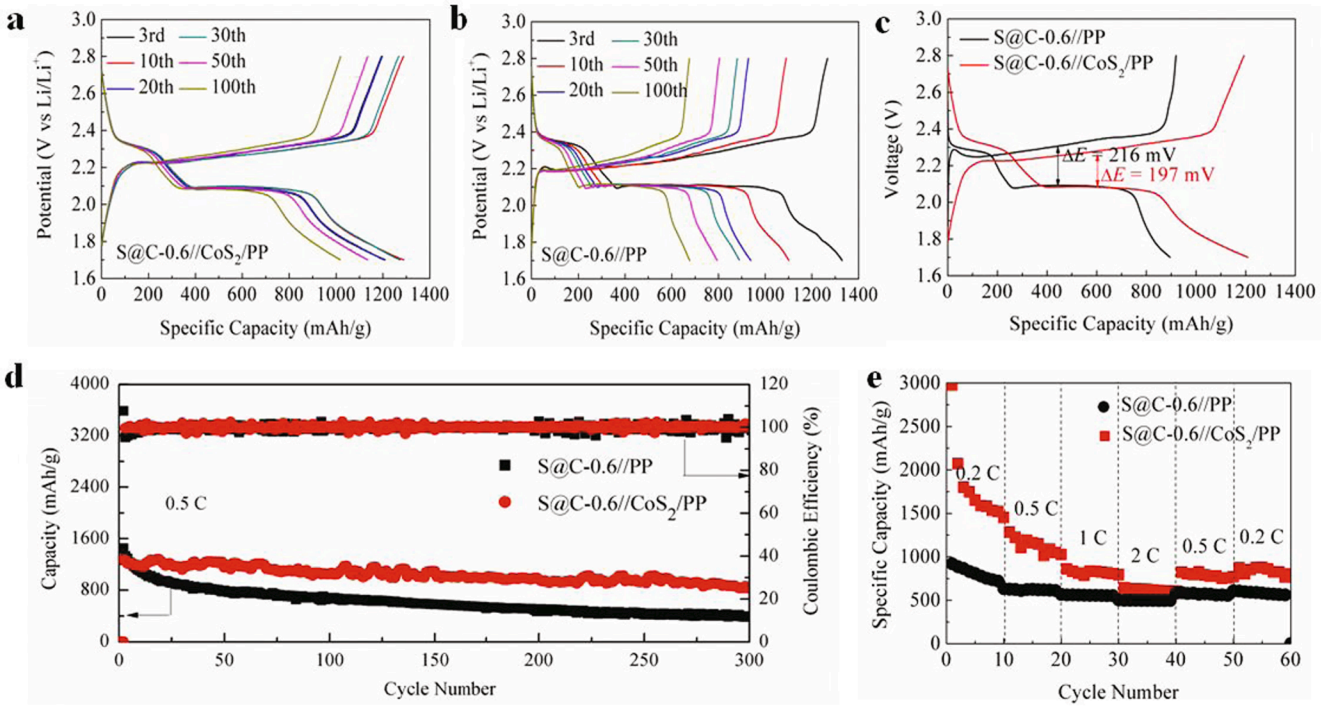

Fig. 5. (a, b) GCD profiles of Li-S batteries S@C-0.6//CoS_2/PP and S@C-0.6//PP at 0.5 C. (c) GCD profiles of Li-S batteries S@C-0.6//CoS_2/PP and S@C-0.6//PP at 0.5 C in the third cycle. (d) Long-term cycling performance of Li-S batteries S@C-0.6//CoS_2/PP and S@C-0.6//PP. (e) The rate capability of Li-S batteries S@C-0.6//CoS_2/PP and S@C-0.6//PP.

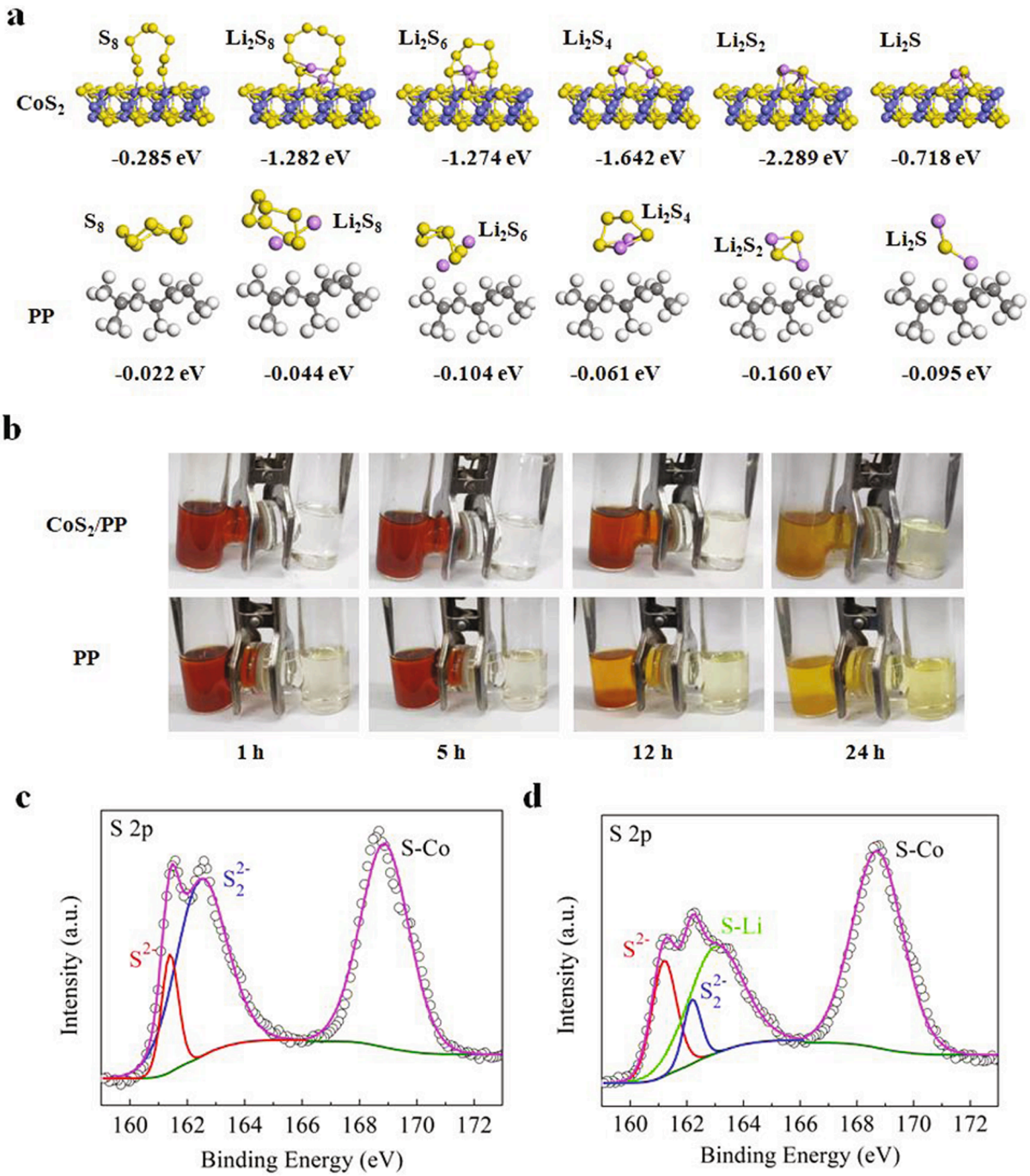

Fig. 6. (a) The adsorption geometries and adsorption energies of polysulfides on CoS_2 surface and PP segments. (b) Polysulfide permeation experiments for Li_2S_6 diffusion across the CoS_2/PP and PP separators from Li_2S_6/THF solution (left side) to pure THF (right side) of the U-shaped glass cell. (c,d) S 2p XPS spectra of CoS_2 before and after soaking in the Li_2S_6/THF solution.

enhancement for Li-S batteries.

4. Conclusions

In summary, we developed an efficient polysulfide double-blocking strategy that simultaneously applied the S@C cathode and MOF derived CoS_2 interlayer to achieve high-performance Li-S batteries. Using the in-situ oxidation method, the elemental S could be evenly confined in the porous carbon and reach to the high loading as 71%. Meanwhile, the CoS_2 interlayer displayed strong chemisorption for polysulfides by forming chemical bonds, which effectively mitigates the shuttling effect. As a consequence, the battery with S@C cathode and CoS_2 interlayer shows superior cycling performance with only 0.136% capacity fading per cycle at 0.5 C. It is confirmed that the synergy of in-situ formed S@C cathode and CoS_2 interlayer on PP separator can effectively anchor the polysulfides and improve the cell cycling stability, which would shed light on the direction of superior Li-S, Li-Se and other metal-S/Se batteries.

CRediT authorship contribution statement

Pengfei Lu: Data curation, Writing - original draft, Formal analysis, Writing - review & editing. **Haodong Shi:** Conceptualization, Methodology, Software. **Jieqiong Qin:** Visualization. **Zhong-Shuai Wu:**

Supervision.

Declaration of Competing Interest

The authors declare that they have no known competing financial interests or personal relationships that could have appeared to influence the work reported in this paper.

Acknowledgements

This work was financially supported by the National Key R&D Program of China (Grants 2016YBF0100100, 2016YFA0200200), National Natural Science Foundation of China (Grants 51872283, 21805273, 22075279, 22005297, 22005298), Liaoning BaiQianWan Talents Program, Natural Science Foundation of Liaoning Province, Joint Research Fund Liaoning-Shenyang National Laboratory for Materials Science (Grant 20180510038), LiaoNing Revitalization Talents Program (Grant XLYC1807153), DICP (DICP ZZBS201708, DICP ZZBS201802, DICP I202032), DNL Cooperation Fund, CAS (DNL180310, DNL180308, DNL201912, and DNL201915), DICP&QIBEBT (Grant DICP&QIBEBT UN201702).

References

[1] Z.-W. Zhang, H.-J. Peng, M. Zhao, J.-Q. Huang, Heterogeneous/homogeneous mediators for high-energy-density lithium-sulfur batteries: progress and prospects, Adv. Funct. Mater. 28 (38) (2018) 1707536.
[2] N. Zhang, Y. Dong, M. Jia, X.u. Bian, Y. Wang, M. Qiu, J. Xu, Y. Liu, L. Jiao, F. Cheng, Rechargeable aqueous Zn–V_2O_5 battery with high energy density and long cycle life, ACS Energy Lett. 3 (6) (2018) 1366–1372.
[3] C. Xia, C.Y. Kwok, L.F. Nazar, A high-energy-density lithium-oxygen battery based on a reversible four-electron conversion to lithium oxide, Science 361 (6404) (2018) 777–781.
[4] Q. Pang, C.Y. Kwok, D. Kundu, X. Liang, L.F. Nazar, Lightweight metallic MgB_2 mediates polysulfide redox and promises high-energy-density lithium-sulfur batteries, Joule 3 (1) (2019) 136–148.
[5] U.-H. Kim, D.-W. Jun, K.-J. Park, Q. Zhang, P. Kaghazchi, D. Aurbach, D.T. Major, G. Goobes, M. Dixit, N. Leifer, C.M. Wang, P. Yan, D. Ahn, K.-H. Kim, C.S. Yoon, Y.-K. Sun, Pushing the limit of layered transition metal oxide cathodes for high-energy density rechargeable Li ion batteries, Energy Environ. Sci. 11 (5) (2018) 1271–1279.
[6] J. Deng, W.-B. Luo, X. Lu, Q. Yao, Z. Wang, H.K. Liu, H. Zhou, S.X. Dou, High energy density sodium-ion battery with industrially feasible and air-stable O3-type layered oxide cathode, Adv. Energy Mater. 8 (2018) 1701610.
[7] L. Zhang, M. Ling, J. Feng, L. Mai, G. Liu, J. Guo, The synergetic interaction between $LiNO_3$ and lithium polysulfides for suppressing shuttle effect of lithium-sulfur batteries, Energy Storage Mater. 11 (2018) 24–29, https://doi.org/10.1016/j.ensm.2017.09.001.
[8] G. Li, Z. Chen, J. Lu, Lithium-sulfur batteries for commercial applications, Chem 4 (1) (2018) 3–7, https://doi.org/10.1016/j.chempr.2017.12.012.
[9] G. Li, S. Wang, Y. Zhang, M. Li, Z. Chen, J. Lu, Revisiting the role of polysulfides in lithium-sulfur batteries, Adv. Mater. 30 (2018) 1705590.
[10] X. Fan, W. Sun, F. Meng, A. Xing, J. Liu, Advanced chemical strategies for lithium–sulfur batteries: a review, Green Energy Environ. 3 (1) (2018) 2–19, https://doi.org/10.1016/j.gee.2017.08.002.
[11] W. Bao, L. Liu, C. Wang, S. Choi, D. Wang, G. Wang, Facile synthesis of crumpled nitrogen-doped mxene nanosheets as a new sulfur host for lithium-sulfur batteries, Adv. Energy Mater. 8 (2018) 1702485.
[12] L. Hu, C. Dai, H. Liu, Y. Li, B. Shen, Y. Chen, S.J. Bao, M. Xu, Double-shelled NiO-$NiCo_2O_4$ heterostructure@carbon hollow nanocages as an efficient sulfur host for advanced lithium-sulfur batteries, Adv. Energy Mater. 8 (2018) 1800709.
[13] J. Zhang, Z. Li, Y.e. Chen, S. Gao, X.W.D. Lou, Nickel-iron layered double hydroxide hollow polyhedrons as a superior sulfur host for lithium-sulfur batteries, Angew. Chem. Int. Ed. 57 (34) (2018) 10944–10948.
[14] L. Hu, C. Dai, J.-M. Lim, Y. Chen, X. Lian, M. Wang, Y.i. Li, P. Xiao, G. Henkelman, M. Xu, A highly efficient double-hierarchical sulfur host for advanced lithium–sulfur batteries, Chem. Sci. 9 (3) (2018) 666–675.
[15] X. Zhu, W. Zhao, Y. Song, Q. Li, F. Ding, J. Sun, L. Zhang, Z. Liu, In situ assembly of 2D conductive vanadium disulfide with graphene as a high-sulfur-loading host for lithium-sulfur batteries, Adv. Energy Mater. 8 (2018) 1800201.
[16] R. Ummethala, M. Fritzsche, T. Jaumann, J. Balach, S. Oswald, R. Nowak, N. Sobczak, I. Kaban, M.H. Rümmeli, L. Giebeler, Lightweight, free-standing 3D interconnected carbon nanotube foam as a flexible sulfur host for high performance lithium-sulfur battery cathodes, Energy Storage Mater. 10 (2018) 206–215, https://doi.org/10.1016/j.ensm.2017.04.004.
[17] M. Kim, H.M. Hwang, G.H. Park, H. Lee, Graphene-based composite electrodes for electrochemical energy storage devices: recent progress and challenges, FlatChem 6 (2017) 48–76.
[18] A. Sanati, K. Raeissi, F. Karimzadeh, A cost-effective and green-reduced graphene oxide/polyurethane foam electrode for electrochemical applications, FlatChem 20 (2020), 100162.
[19] M. Ding, F.-H. Du, B.o. Liu, Z.Y. Leong, L.u. Guo, F. Chen, A. Baji, H.Y. Yang, Rod-like nitrogen-doped carbon hollow shells for enhanced capacitive deionization, FlatChem 7 (2018) 10–17, https://doi.org/10.1016/j.flatc.2018.01.002.
[20] Q. Pang, X. Liang, C.Y. Kwok, L.F. Nazar, Advances in lithium-sulfur batteries based on multifunctional cathodes and electrolytes, Nat. Energy 1 (2016) 16132.
[21] Z. Li, J. Zhang, B. Guan, D. Wang, L.M. Liu, X.W. Lou, A sulfur host based on titanium monoxide@carbon hollow spheres for advanced lithium-sulfur batteries, Nat. Commun. 7 (2016) 13065.
[22] Z. Li, J. Zhang, X.W.D. Lou, Hollow carbon nanofibers filled with MnO_2 nanosheets as efficient sulfur hosts for lithium-sulfur batteries, Angew. Chem. Int. Ed. 54 (44) (2015) 12886–12890, https://doi.org/10.1002/anie.201506972.
[23] X. Tao, J. Wang, C. Liu, H. Wang, H. Yao, G. Zheng, Z.W. Seh, Q. Cai, W. Li, G. Zhou, C. Zu, Y. Cui, Balancing surface adsorption and diffusion of lithium-polysulfides on nonconductive oxides for lithium-sulfur battery design, Nat. Commun. 7 (2016) 11203.
[24] S. Wang, H. Chen, J. Liao, Q. Sun, F. Zhao, J. Luo, X. Lin, X. Niu, M. Wu, R. Li, X. Sun, Efficient trapping and catalytic conversion of polysulfides by VS_4 nanosites for Li–S batteries, ACS Energy Lett. 4 (3) (2019) 755–762, https://doi.org/10.1021/acsenergylett.9b00076.s001.
[25] C. Ye, L. Zhang, C. Guo, D. Li, A. Vasileff, H. Wang, S.Z. Qiao, A 3D hybrid of chemically coupled nickel sulfide and hollow carbon spheres for high performance lithium-sulfur batteries, Adv. Funct. Mater. 27 (2017) 1702524.
[26] Z. Yuan, H.-J. Peng, T.-Z. Hou, J.-Q. Huang, C.-M. Chen, D.-W. Wang, X.-B. Cheng, F. Wei, Q. Zhang, Powering lithium–sulfur battery performance by propelling polysulfide redox at sulfiphilic hosts, Nano Lett. 16 (1) (2016) 519–527, https://doi.org/10.1021/acs.nanolett.5b04166.s001.
[27] J. Zhou, N. Lin, W.L. Cai, C. Guo, K. Zhang, J. Zhou, Y. Zhu, Y. Qian, Synthesis of S/CoS_2 nanoparticles-embedded N-doped carbon polyhedrons from polyhedrons ZIF-67 and their properties in lithium-sulfur batteries, Electrochim. Acta 218 (2016) 243–251, https://doi.org/10.1016/j.electacta.2016.09.130.
[28] H. Wang, W. Zhang, J. Xu, Z. Guo, Advances in polar materials for lithium-sulfur batteries, Adv. Funct. Mater. 28 (2018) 1707520.
[29] Y. Dong, P. Lu, H. Shi, J. Qin, J. Chen, W. Ren, H.-M. Cheng, Z.-S. Wu, 2D hierarchical yolk-shell heterostructures as advanced host-interlayer integrated electrode for enhanced Li-S batteries, J. Energy Chem. 36 (2019) 64–73.
[30] Z. Xia, Q. Huang, S. Guo, Recent progress on synthesis, structure and electrocatalytic applications of MXenes, FlatChem 17 (2019), 100129.
[31] T. Zhou, W. Lv, J. Li, G. Zhou, Y. Zhao, S. Fan, B. Liu, B. Li, F. Kang, Q.-H. Yang, Twinborn TiO_2–TiN heterostructures enabling smooth trapping–diffusion–conversion of polysulfides towards ultralong life lithium–sulfur batteries, Energy Environ. Sci. 10 (7) (2017) 1694–1703.
[32] D.-R. Deng, F. Xue, Y.-J. Jia, J.-C. Ye, C.-D. Bai, M.-S. Zheng, Q.-F. Dong, Co_4N nanosheet assembled mesoporous sphere as a matrix for ultrahigh sulfur content lithium–sulfur batteries, ACS Nano 11 (6) (2017) 6031–6039, https://doi.org/10.1021/acsnano.7b01945.s001.
[33] L. Ma, H. Yuan, W. Zhang, G. Zhu, Y. Wang, Y.i. Hu, P. Zhao, R. Chen, T. Chen, J. Liu, Z. Hu, Z. Jin, Porous-shell vanadium nitride nanobubbles with ultrahigh areal sulfur loading for high-capacity and long-life lithium–sulfur batteries, Nano Lett. 17 (12) (2017) 7839–7846.
[34] G. Jiang, F. Xu, S. Yang, J. Wu, B. Wei, H. Wang, Mesoporous, conductive molybdenum nitride as efficient sulfur hosts for high-performance lithium-sulfur batteries, J. Power Sources 395 (2018) 77–84.
[35] Y. Zheng, X. Li, C. Pi, H. Song, B. Gao, P.K. Chu, K. Huo, Recent advances of two-dimensional transition metal nitrides for energy storage and conversion applications, FlatChem 19 (2020), 100149.
[36] T. Lei, W. Chen, Y. Hu, W. Lv, X. Lv, Y. Yan, J. Huang, Y. Jiao, J. Chu, C. Yan, C. Wu, Q. Li, W. He, J. Xiong, A nonflammable and thermotolerant separator suppresses polysulfide dissolution for safe and long-cycle lithium-sulfur batteries, Adv. Energy Mater. 8 (2018) 1802441.
[37] S. Wang, F. Gao, Y. Zhao, N. Liu, T. Tan, X. Wang, Two-dimensional CeO_2/RGO composite-modified separator for lithium/sulfur batteries, Nanoscale Res. Lett. 13 (2018) 13377.
[38] S.H. Kim, J.S. Yeon, R. Kim, K.M. Choi, H.S. Park, A functional separator coated with sulfonated metal–organic framework/Nafion hybrids for Li–S batteries, J. Mater. Chem. A 6 (48) (2018) 24971–24978, https://doi.org/10.1039/C8TA08843H.
[39] T. Lei, W. Chen, W. Lv, J. Huang, J. Zhu, J. Chu, C. Yan, C. Wu, Y. Yan, W. He, J. Xiong, Y. Li, C. Yan, J.B. Goodenough, X. Duan, Inhibiting polysulfide shuttling with a graphene composite separator for highly robust lithium-sulfur batteries, Joule 2 (10) (2018) 2091–2104, https://doi.org/10.1016/j.joule.2018.07.022.
[40] L. Wang, Y.-B. He, L.u. Shen, D. Lei, J. Ma, H. Ye, K. Shi, B. Li, F. Kang, Ultra-small self-discharge and stable lithium-sulfur batteries achieved by synergetic effects of multicomponent sandwich-type composite interlayer, Nano Energy 50 (2018) 367–375, https://doi.org/10.1016/j.nanoen.2018.05.043.
[41] Y.C. Jeong, J.H. Kim, S. Nam, C.R. Park, S.J. Yang, Rational design of nanostructured functional interlayer/separator for advanced Li-S batteries, Adv. Funct. Mater. 28 (2018) 1707411.
[42] J.-Q. Huang, T.-Z. Zhuang, Q. Zhang, H.-J. Peng, C.-M. Chen, F. Wei, Permselective graphene oxide membrane for highly stable and anti-self-discharge lithium–sulfur batteries, ACS Nano 9 (3) (2015) 3002–3011, https://doi.org/10.1021/nn507178a.

[43] L. Yin, G. Xu, P. Nie, H. Dou, X. Zhang, MXene debris modified eggshell membrane as separator for high-performance lithium-sulfur batteries, Chem. Eng. J. 352 (2018) 695–703, https://doi.org/10.1016/j.cej.2018.07.063.
[44] H. Yao, K. Yan, W. Li, G. Zheng, D. Kong, Z.W. Seh, V.K. Narasimhan, Z. Liang, Y. i. Cui, Improved lithium–sulfur batteries with a conductive coating on the separator to prevent the accumulation of inactive S-related species at the cathode–separator interface, Energy Environ. Sci. 7 (10) (2014) 3381–3390, https://doi.org/10.1039/C4EE01377H.
[45] J. Balach, H.K. Singh, S. Gomoll, T. Jaumann, M. Klose, S. Oswald, M. Richter, J. Eckert, L. Giebeler, Synergistically enhanced polysulfide chemisorption using a flexible hybrid separator with N and S dual-doped mesoporous carbon coating for advanced lithium–sulfur batteries, ACS Appl. Mater. Interfaces 8 (23) (2016) 14586–14595, https://doi.org/10.1021/acsami.6b03642.s001.
[46] Z. Sun, S. Vijay, H.H. Heenen, A.Y.S. Eng, W. Tu, Y. Zhao, S.W. Koh, P. Gao, Z. W. Seh, K. Chan, H. Li, Catalytic polysulfide conversion and physiochemical confinement for lithium-sulfur batteries, Adv. Energy Mater. 10 (2020) 1904010.
[47] G. Li, J. Sun, W. Hou, S. Jiang, Y. Huang, J. Geng, Three-dimensional porous carbon composites containing high sulfur nanoparticle content for high-performance lithium-sulfur batteries, Nat. Commun. 7 (2016) 10601.
[48] H. Shi, X. Zhao, Z.-S. Wu, Y. Dong, P. Lu, J. Chen, W. Ren, H.-M. Cheng, X. Bao, Free-standing integrated cathode derived from 3D graphene/carbon nanotube aerogels serving as binder-free sulfur host and interlayer for ultrahigh volumetric-energy-density lithium sulfur batteries, Nano Energy 60 (2019) 743–751, https://doi.org/10.1016/j.nanoen.2019.04.006.
[49] Y. Dong, W. Shi, P. Lu, J. Qin, S. Zheng, B. Zhang, X. Bao, Z.-S. Wu, 2D holey cobalt sulfide nanosheets derived from metal–organic frameworks for high-rate sodium ion batteries with superior cyclability, J. Mater. Chem. A 6 (29) (2018) 14324–14329, https://doi.org/10.1039/C8TA05612A.
[50] G. Kresse, J. Hafner, Ab initio molecular dynamics for liquid metals, Phys. Rev. B 47 (1) (1993) 558–561, https://doi.org/10.1103/PhysRevB.47.558.
[51] G. Kresse, J. Hafner, Ab initio molecular-dynamics simulation of the liquid-metal–amorphous-semiconductor transition in germanium, Phys. Rev. B 49 (20) (1994) 14251–14269, https://doi.org/10.1103/PhysRevB.49.14251.
[52] J.P. Perdew, K. Burke, M. Ernzerhof, Generalized gradient approximation made simple, Phys. Rev. Lett. 77 (18) (1996) 3865–3868, https://doi.org/10.1103/PhysRevLett.77.3865.
[53] J.A. White, D.M. Bird, Implementation of gradient-corrected exchange-correlation potentials in Car-Parrinello total-energy calculations, Phys. Rev. B 50 (7) (1994) 4954–4957, https://doi.org/10.1103/PhysRevB.50.4954.
[54] H.J. Monkhorst, J.D. Pack, Special points for Brillouin-zone integrations, Phys. Rev. B 13 (12) (1976) 5188–5192, https://doi.org/10.1103/PhysRevB.13.5188.
[55] X. Hong, S. Li, X. Tang, Z. Sun, F. Li, Self-supporting porous CoS_2/rGO sulfur host prepared by bottom-up assembly for lithium-sulfur batteries, J. Alloys Compounds 749 (2018) 586–593, https://doi.org/10.1016/j.jallcom.2018.03.331.
[56] X. Liu, J.Q. Huang, Q. Zhang, L. Mai, Nanostructured metal oxides and sulfides for lithium-sulfur batteries, Adv. Mater. 29 (2017) 1601759.
[57] F. Yin, J. Ren, Y. Zhang, T. Tan, Z. Chen, A PPy/ZnO functional interlayer to enhance electrochemical performance of lithium/sulfur batteries, Nanoscale Res. Lett. 13 (2018) 13307.
[58] X. Yu, G. Zhou, Y.i. Cui, Mitigation of shuttle effect in Li–S battery using a self-assembled ultrathin molybdenum disulfide interlayer, ACS Appl. Mater. Interfaces 11 (3) (2019) 3080–3086, https://doi.org/10.1021/acsami.8b19354.s001.
[59] H. Shi, Y. Dong, F. Zhou, J. Chen, Z.S. Wu, 2D hybrid interlayer of electrochemically exfoliated graphene and $Co(OH)_2$ nanosheet as a bi-functionalized polysulfide barrier for high-performance lithium-sulfur batteries, J. Phys. Energy 1 (2018), 015002.